North Carolina Journal of
Mathematics and Statistics
Volume 8, Pages 15–31 (Accepted October 15, 2022, published October 22, 2022)
ISSN 2380-7539

Mathematical analysis of tumor-immune interactions based on Michaelis-Menten kinetics with CAR-T immunotherapy

ERIK J. XIE, HARISH RAMASAMY, AND WEI FENG

ABSTRACT. In this paper, we study the dynamics of tumor growth under immune system surveillance with a mathematical model based on Michaelis-Menten kinetics. In our three-component differential equation system, we accounted for the factor of immunotherapy, its effect on tumor population, and synergy with immune cells. CAR-T, or Chimeric Antigen Receptor T cell, therapy is chosen to be incorporated into the model as a form of immunotherapy due to its promising clinical applications. The stability of the steady-state equilibria of the system is analyzed with parameters from referred sources, and the various patterns of dynamics are demonstrated through numerical simulations. The analysis shows different outcomes of the tumor population given different parameters and initial values, which provides insights into the clinical practicability of CAR-T treatment. Earlier stages of tumor progression at which therapy begins, a critical time frame of therapeutic injection to prevent tumor relapse, and improvement of antigen affinity of the receptors are found to be factors that can enhance CAR-T efficiency and cancer patients' life span. For further analysis, we also propose an expanded system to investigate the potential off-target toxic effects of CAR-T cells on normal host cells. Our instability results and oscillating numerical patterns suggest non-cooperation between the cell types, posing potential clinical challenges to the therapy.

1. Introduction

As the second leading cause of death in the United States (CDC, 2022), cancer threatens the lives of more than 1.7 million people each year. Tumors cells that proliferate excessively are the underlying cause of cancer, and when tumor cells are detected in the body, the immune system responds by deploying $CD8^+$ cytotoxic T cells to inhibit tumor proliferation (Mahlbacher et al., 2019). However, because tumor cells, such as those in solid tumors, have defense mechanisms that resist host immunity (Bahrambeigi et al., 2019), in many cases, the tumor gains malignancy and metastasizes by overcoming or evading the immune system actions (Marino-Enriquez and Fletcher, 2014). While the host immune system is unable to exert its full strength in many cases, it does have complicated processes to control neoplastic cell growth (Uehara et al., 2019). Different mathematical models have also been proposed to study these interactions over the past century, describing the dynamics between populations such as host, tumor, and immune cells (Das et al., 2020); and cytokines and antigens. Different types of therapies, such as immune-checkpoint inhibitors, have also been modeled in terms of their impact on immune activation and tumor control (Queirolo et al., 2019).

Due to the difficulty of controlling cancer growth, immunotherapies have been developed with the intent to induce stronger anti-tumor responses by the host immune system, and in this study, we

Received by the editors August 28, 2022.
2010 *Mathematics Subject Classification.* 92B05; 34A34.
Key words and phrases. tumor-immune, immunotherapy, CAR-T, Michaelis-Menten, Mathematical biology.

consider immunotherapy as an extra factor besides the tumor-immune interactions due to interests in their effectiveness. One promising form of immunotherapy is the recently developed Chimeric Antigen Receptor T cells (CAR-T cells), which are genetically engineered lymphocytic cells used to kill tumor cells in the body. The genome of the lymphocyte receives in vitro injection of CAR genes to express the desired antigen receptor specific to $CD19^+$ antigens expressed by tumor cells growing in the host (Pérez-García et al., 2021). After clinical progress in recent years, CAR-T cells are currently applied to treat lymphomas, acute myeloid leukemia, and multiple myeloma after approval by the FDA in 2017. The focus of this paper is to perform an analysis of the interaction of CAR-T cells with its target tumor cells and the host immune system.

2. Equations

A Michaelis-Menten based system describing the interaction between immune cells, tumor cells, and host cells has been proposed by Das et al. (2020). The model presents as follows:

$$\frac{dH}{dt} = \alpha H\left(1 - \frac{H}{K_1}\right) - \gamma_1 TH \tag{2.1}$$

$$\frac{dI}{dt} = \frac{n_1 TI}{\kappa_1 + T} - \delta TI - \rho I \tag{2.2}$$

$$\frac{dT}{dt} = \beta T\left(1 - \frac{T}{K_2}\right) - \gamma_2 TH - \frac{n_2 TI}{\kappa_2 + T}, \tag{2.3}$$

where H, I, and T represent the host cell population, the immune cell population, and the tumor cell population, respectively. In this system, the host cell population follows a logistic growth model with a carrying capacity of K_1 and experiences inactivation by tumor cells at rate γ_1. The immune cell population is assumed to interact with tumor cells according to Michaelis-Menten kinetics with rate n_1 and stiffness coefficient κ_1. The tumor population grows according to a logistic function with carrying capacity K_2 and is inactivated at rate γ_2 by host cells and n_2 by immune cells.

Another system proposed by Pérez-García et al. (2021) accounts for the dynamics of similar cell populations with the addition of immunotherapy. It presents as follows:

$$\frac{dC}{dt} = \rho_C(T + L + C)C - \frac{1}{\tau_C}C - \alpha C^2 + \rho_1 C \tag{2.4}$$

$$\frac{dL}{dt} = \rho_L L - \alpha LC \tag{2.5}$$

$$\frac{dT}{dt} = g(T, L, C) - \alpha TC, \tag{2.6}$$

where C, L, and T represent the populations of CAR-T cells, tumor cells (leukemic T-cells), and normal T-cells. The CAR-T cell population proliferates at rate ρ_1 and is stimulated at rate ρ_C. The parameter α represents CAR-T fratricide. The leukemic cells grow at rate ρ_L and are inactivated by CAR-T cells at rate α. The normal T cell population is killed by tumor cells at rate α. $g(T, L, C)$ represents the production rate of normal T-cells, which is assumed to be negligible in the original study.

In this study, we propose a different model based on the two previously mentioned studies. The equations describe the rate of change in cell populations of three types: tumor cells (T), immune cells (M), and CAR-T cells (ϕ).

$$\frac{dT}{dt} = \alpha T(\ln \beta - \ln T) - \frac{n_1 T(M+\phi)}{T+\kappa_1} \tag{2.7}$$

$$\frac{dM}{dt} = \frac{n_2 TM}{T+\kappa_2} - p_1 M - K_1 TM \tag{2.8}$$

$$\frac{d\phi}{dt} = p_2 + \frac{n_3 TM}{T+\kappa_3} - \frac{1}{\tau_c}\phi + K_2 \phi M. \tag{2.9}$$

To validate the mathematical model, a couple of assumptions are made about the tumor-immune microenvironment. As represented by the first term of (2.7), it is assumed that the tumor population follows a Gompertzian model that has been used to fit growth data of tumors (Jenner et al., 2019; d'Onofrio et al., 2011). The model differs from the logistic growth model assumed by Das et al. (2020) in the asymmetrically asymptotic behavior of the tumor population. A Michaelis-Menten kinetics-based model is modified from the system proposed by Das et al. (2020) and represented by the second term of (2.7), where it accounts for the clearance of the tumor population by immune and CAR-T cells. Due to the CAR-T cells being an analogous component of the immune cell population, the two populations have been combined by the additive term $(M + \phi)$ in the tumor clearance rate. Used to describe cell interactions in this model, the Michaelis-Menten model was initially adopted to describe enzyme kinetics, and it has also been applied to food chain dynamics where similar interactions with capacities prevail (Holling, 1959; Xie et al., 2021). In this paper and the study by Das et al. (2020), the model is adopted because it describes the interactions between cell types more rigorously compared to a linear model which, unrealistically, represents immune cells with no upper limit to their rate of tumor recognition and destruction (Srinivasan, 2021).

Equation (2.8) represents the rate of change in immune cell population, which we assume to operate as a whole instead of separate components for simplification purposes. More complex models have been proposed and studied in previous research to investigate the dynamics of individual immune components (Mahlbacher et al., 2019). The equation is adopted directly from Das et al. (2020). The immune cells are activated by interacting with tumor cell antigens, and the rate is represented by the first term based on Michaelis-Menten kinetics. The rate of activation is dependent on the antigenicity of the tumor, which is the relative extent to which tumor cells express molecules that are detectable for immune and CAR-T cells. The rate of natural mortality and inactivation by tumor of immune cells are also accounted for in (2.8) by the second and third terms.

The rate of change in CAR-T cell population, represented by ϕ, is modeled by (2.9), where CAR-T cells activate and decay according to their natural life span τ_c, as included in the model by Pérez-García et al. (2021). The constant p_2 accounts of the therapeutic process where CAR-T cells may be injected into the host at constant rates after the initial treatment to prevent tumor relapses, and it is an added term not used in previous studies. The second term is modified from Das et al. (2020) and describes the Michaelis-Menten based synergistic activation of CAR-T cells by tumor and immune cells (Robertson-Tessi et al., 2012). The last terms describes the activation of CAR-T cells by individual immune components, and it is modified from the equation by Pérez-García et al. (2021) by the inclusion of the CAR-T cell population in the term to represent the dependence of

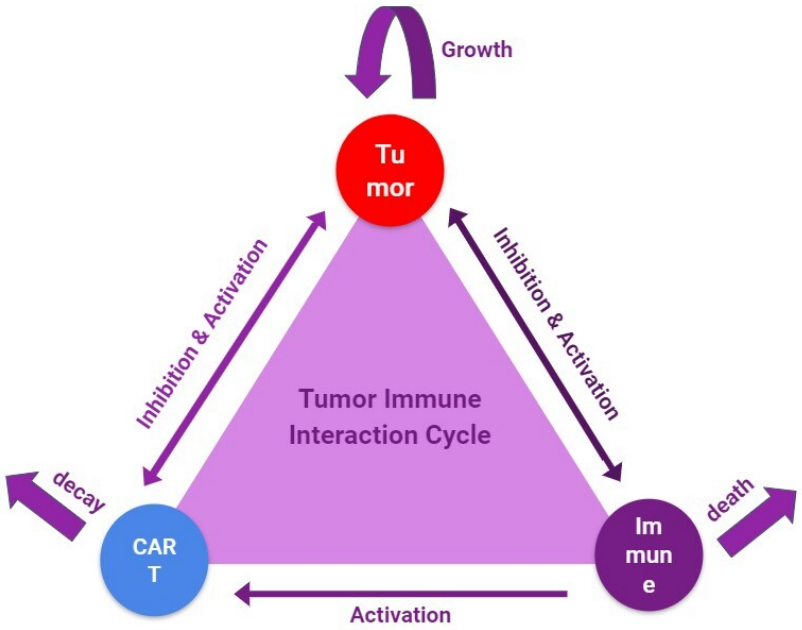

FIGURE 2.1. A diagram illustrating the dynamics of the system. The external input of CAR-T cells is not described in this diagram.

TABLE 2.1. Explanation of variables in the system

Variables	Explanation	Used by
α	The proliferation rate of tumor cells	Jenner et al. (2019)
n_1, n_2, n_3	Rate constants of Michaelis-Menten kinetics	Das et al. (2020)
$\kappa_1, \kappa_2, \kappa_3$	Stiffness coefficients representing half-saturation points	Das et al. (2020)
β	The host tumor carrying capacity	Jenner et al. (2019)
p_1	Natural mortality rate of immune cell	Das et al. (2020)
p_2	Rate of external CAR T cell injection	Original
K_1	Rate of immune cell inhibition by tumor cells	Das et al. (2020)
K_2	Rate of CAR T cell activation by tumor and B cells	Das et al. (2020)
τ_c	Life span of CAR T cells (Pérez-García et al., 2021)	

the rate interaction on the CAR-T cell population size. In Table 2.1, the constants in the differential equations are summarized and explained, and Figure 2.1 presents a schematic representation of the interactions involved in this model.

3. Methods

In table 3.1, the parameters and initial values (T_0, M_0, ϕ_0) used in the numerical simulation of the model are gathered from previously validated research studies and summarized after adjustment. The Michaelis-Menten-based parameters are mostly taken from the Kuznetsov et al. (1994), which included estimated values based on BCL_1 lymphoma in mice. The data for the tumor population is taken and adjusted from previous studies by different authors (Vaghi et al., 2020; Barros et al.,

TABLE 3.1. Parameters used in the model

Variables	Values	Units	Reference
α	0.580	day^{-1}	Vaghi et al. (2020)
n_1	0.1245	day^{-1}	Kuznetsov et al. (1994)
n_2	0.45	day^{-1}	adjusted from Itik and Banks (2010)
n_3	0.15	day^{-1}	adjusted from León-Triana et al. (2021)
κ_1	2.02×10^7	cells	Kuznetsov et al. (1994)
κ_2	3.5×10^7	cells	adjusted from Kuznetsov et al. (1994)
κ_3	5×10^7	cells	León-Triana et al. (2021)
β	2.00×10^9	cells	adjusted from Barros et al. (2021)
p_1	4.20×10^{-2}	day^{-1}	Yates and Callard (2001)
p_2	0	cells $\times$ day^{-1}	estimated
K_1	3.422×10^{-10}	day$^{-1}\times$ cell^{-1}	Kuznetsov et al. (1994)
K_2	2.92×10^{-11}	day$^{-1}\times$ cell^{-1}	Pérez-García et al. (2021)
τ_c	14	days	Pérez-García et al. (2021)

2021), and the parameters relating to CAR-T are adjusted from the values presented in the previously mentioned T-cell leukemia study by Pérez-García et al. (2021). For preliminary analysis, it is assumed that no external input of CAR-T cells ($p_2 = 0$) is applied after the initial injection of CAR-T cells defining $\phi(0)$. The injection rate and its effect on the system will be considered and discussed in the next section.

To linearize the system of differential equations, the Jacobian of the system is obtained by taking the partial derivatives of the differential equations in a 3 by 3 matrix.

$$\textbf{Jacobian} = \begin{bmatrix} \ln\left(\frac{\beta}{T}\right)\alpha - \alpha - \frac{n_1(M+\phi)}{(T+\kappa_1)^2} & \frac{-n_1 T}{T+\kappa_1} & \frac{-n_1 T}{T+\kappa_1} \\ \frac{n_2 M}{T+\kappa_2} - \frac{n_2 TM}{(T+\kappa_2)^2} - K_1 M & \frac{n_2 T}{T+\kappa_2} - p_1 - K_1 T & 0 \\ \frac{n_3 M}{T+\kappa_3} - \frac{n_3 TM}{(T+\kappa_3)^2} & \frac{n_3 T}{T+\kappa_3} + K_2\phi & \frac{-1}{\tau_c} + K_2 M \end{bmatrix}. \tag{3.1}$$

The steady-state coordinates of the system are obtained computationally using Maple, a mathematical analysis software, and the data parameters are taken and estimated from cited sources. The equilibria correspond to the points at which $\frac{dT}{dt} = \frac{dM}{dt} = \frac{d\phi}{dt} = 0$, where none of the three populations is changing (Edelstein-Keshet, 2005). After excluding the equilibria involving negative or imaginary values, the biologically relevant solutions are listed as follow and analyzed for stability.

$$\text{(I)}\{T = 2.000 \times 10^9, M = 0, \phi = 0\} \tag{3.2}$$

$$\text{(II)}\{T = 3.723 \times 10^6, M = 2.381 \times 10^8, \phi = 1.503 \times 10^8\} \tag{3.3}$$

$$\text{(III)}\{T = 1.161 \times 10^9, M = 4.647 \times 10^8, \phi = 1.195 \times 10^9\} \tag{3.4}$$

By evaluating the Jacobian matrix using the steady-state coordinates and the constant parameters in Table 3.1, the eigenvalues for equilibrium (I) are calculated from the characteristic polynomial

$$P_1(A) = A^3 + .931A^2 + .224A + .0116 \tag{3.5}$$

and stored in matrix

$$\mathbf{A_1} = \begin{bmatrix} -0.580 \\ -0.280 \\ -0.0714 \end{bmatrix}. \tag{3.6}$$

This equilibrium represents the tumor population reaching its carrying capacity and the immune components being correspondingly eliminated. No coexistence between the cell populations is achieved in this scenario. The equilibrium is asymptotically stable based on the negative values of the eigenvalues. Biologically, the host is in an unhealthy state (or deceased) at this equilibrium, where the tumor has out-competed the immune system and CAR-T therapy and potentially metastasized.

For equilibrium (II), the eigenvalues are obtained in a similar manner from the characteristic polynomial

$$P_2(A) = A^3 + 0.0768A^2 + 0.152A + 0.00927 \tag{3.7}$$

and shown in matrix

$$\mathbf{A_2} = \begin{bmatrix} -0.00766 + 0.388i \\ -0.0615 \\ -0.00766 - 0.388i \end{bmatrix}. \tag{3.8}$$

This equilibrium shows the suppression of tumor growth by the immune system, aided by CAR-T cells; the tumor population is significantly below its maximum threshold, and the immune and CAR-T cells maintain their population. This steady-state is indicative of the therapeutic effects of CAR-T cells, which combine with immune cells to suppress tumors at a level three degrees of magnitude below their carrying capacity (about 0.186 % of it). The equilibrium is asymptotically stable as $\Re(A_2)$ is uniformly negative, and the three populations are able to coexist at equilibrium (II).

For the last equilibrium, the characteristic polynomial of the Jacobian is

$$P_3(A) = A^3 + 0.328A^2 - 0.0180A - 0.00815. \tag{3.9}$$

The eigenvalues of equilibrium (III) are shown in matrix

$$\mathbf{A_3} = \begin{bmatrix} 0.151 \\ -0.183 \\ -0.296 \end{bmatrix}. \tag{3.10}$$

Rather than showing stability, this equilibrium is a saddle point because of the mixed signs of the eigenvalues. The biological explanation of this equilibrium is that the immune system cannot maintain stable levels under the dominance of the tumor population due to the inhibitory effects, as the level of immune cells is substantially lower than that of the tumor cells at this equilibrium. When immune cells are significantly out-competed, the CAR-T cells cannot suppress the tumor population on their own despite having a population size comparable to that of the tumor.

Overall, two stable nodes are obtained based on the system of equation (I)-(III), and one unstable node is obtained as a saddle point. No trivial steady-state involving all three populations going to extinction ($T = 0, M = 0, \phi = 0$) is obtained, as (2.7) would be undefined given $T = 0$. In the next section, simulations of the behavior of the system are conducted using initial values, and different patterns corresponding to the equilibrium nodes are observed and analyzed.

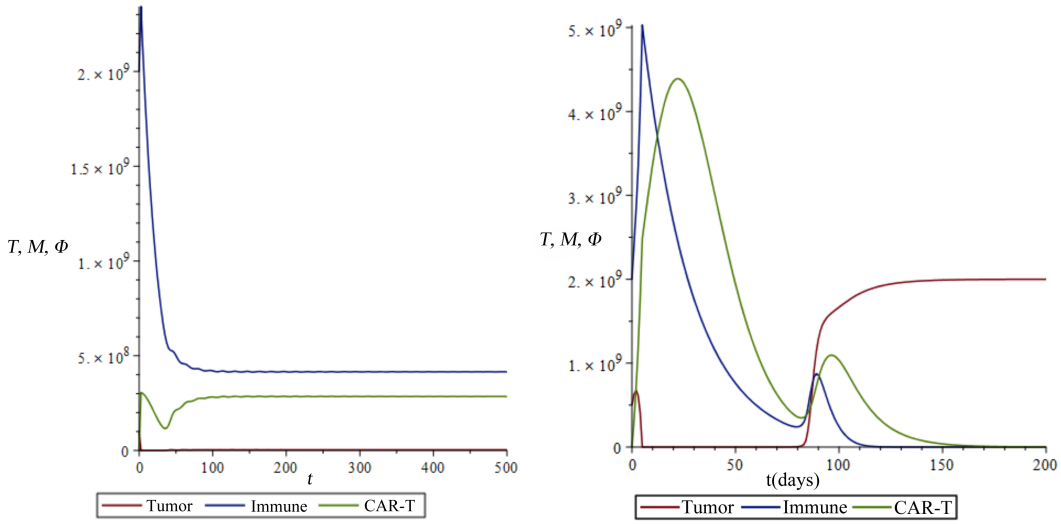

FIGURE 4.1. Tumor-immune dynamics. Left: Using $T(0) = 10^8, M(0) = 2 \times 10^9, \phi(0) = 10^9$, our simulation graph shows tumor suppression by immune and CAR-T cells beginning shortly after $t = 0$. Right: Using $T(0) = 5 \times 10^8, M(0) = 2 \times 10^9, \phi(0) = 10^9$, our simulation graph shows tumor dominating over immune and CAR-T cells after a time period of approximately 80 days.

4. Results

4.1. Analysis of Initial Values

We now conduct numerical simulations of the model using different initial data and parameters in order to visualize and interpret the behavior of the three populations. By changing the initial tumor population and keeping the other parameters and initial conditions constant, different outcomes can be observed. The outcome in Figure 4.1 corresponds to equilibrium (I), where the tumor population starts with 5×10^8 cells and eventually reaches the attractor steady-state of 2.00×10^9 cells where the system achieves stability. Figure 4.1 corresponds to equilibrium (II), which is also stable with a very low tumor population persisting under immune surveillance. With initial values of immune and CAR-T cells kept constant, a qualitative bifurcation is observed at an initial tumor population of around 4.8×10^8 cells, where the system switches between the two equilibria shown in Figures 4.1. The initial tumor size is comparable to the progress of the disease in the host; the observation that the tumor is nearly eliminated when it starts with a relatively small population of 10^8 cells, while it is able to persist when starting with a larger population of 5×10^8 cells, provides the biological explanation that the CAR-T therapy is more effectively combined with the immune system at an earlier stage of tumor development. Since the rate of tumor development is approximately exponential before the population reaches about half of its carrying where an inflection occurs, an earlier stage treatment could mean a significantly lower starting tumor population and vice versa. Figure 4.2 is a 3D visualization of the trajectory taken by the system under two different initial conditions.

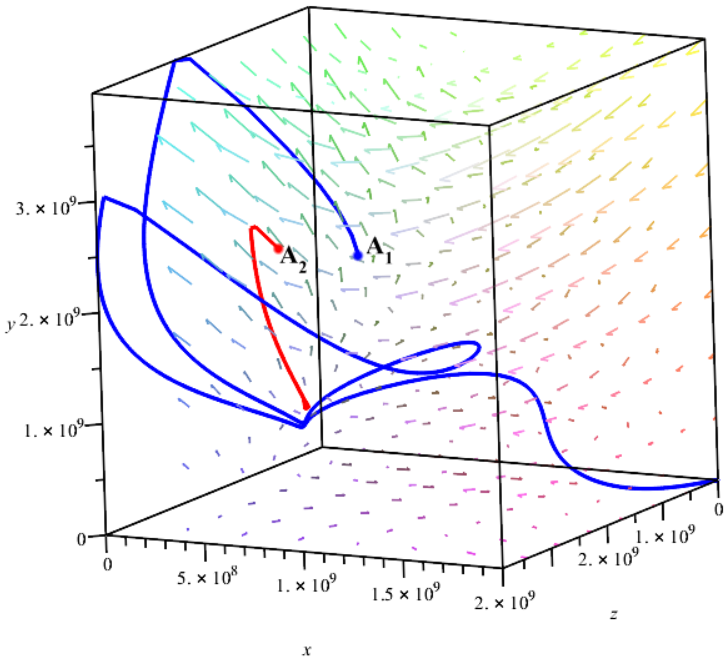

FIGURE 4.2. Phase portrait of tumor, immune, and CAR-T cell interactions. The 3D vector field represents one of the steady-state coordinates of the system. The initial conditions are $A_1 = \{T(0) = 5 \times 10^8, M(0) = 2 \times 10^9, \phi(0) = 10^9\}$ and $A_2 = \{T(0) = 10^8, M(0) = 2 \times 10^9, \phi(0) = 10^9\}$, where A_1 eventually reaches the tumor dominant equilibrium and A_2 the suppressed equilibrium.

4.2. Bifurcation of Initial Values

It is noted that a bifurcation occurs in the system at certain initial values. In this section, we consider the impact of initial tumor and immune populations on the outcome of the system, while maintaining $\phi(0)$ constant at $1.0 \cdot 10^9$ cells. When the initial tumor and immune cell populations are at comparable levels (10^8 cells), the convergence to steady-state II, where the tumor population is suppressed, is observed only when the immune cell population begins at levels above a certain threshold. The points in table 4.1 with 0.5 increments represent the convergence of the system given different sets of initial conditions above and below the bifurcation point. Both asymptotically stable steady-states I and II are observed, but the latter occurs at M(0) above the threshold for each different initial tumor population, and the former at M(0) below it. Minimal CAR-T therapeutic effects are observed as the tumor proliferates rapidly under conditions that lead to the convergence to steady-state I.

When the immune cell population begins at levels much higher than the tumor cell population (10^9 cells), the bifurcation between the two steady-states is observed with a different pattern, where the system converges to steady-state II when the initial immune cell population is below the bifurcation point, and to steady-state I when the initial immune cell population is above it. Table 4.2 demonstrates this behavior with sets of initial conditions with 0.5 increments. With a immune cell population starting at levels out of the range that leads to convergence to steady-state II, the tumor will be uncontrolled and eventually reach its carrying capacity.

TABLE 4.1. Bifurcation points of tumor immune dynamics

$10^{-8}\cdot$ T(0)	$10^{-8}\cdot$ M(0)	$10^{-9}\cdot\phi$(0)	Convergence to Steady-State
1.0	3.0	1.0	I
1.0	3.5	1.0	II
1.5	3.5	1.0	I
1.5	4.0	1.0	II
2.0	4.5	1.0	I
2.0	5.0	1.0	II
2.5	4.5	1.0	I
2.5	5.0	1.0	II
3.0	5.5	1.0	I
3.0	6.0	1.0	II
3.5	5.5	1.0	I
3.5	6.0	1.0	II
4.0	6.5	1.0	I
4.0	7.0	1.0	II

TABLE 4.2. Bifurcation points of tumor immune dynamics

$10^{-8}\cdot$ T(0)	$10^{-9}\cdot$ M(0)	$10^{-9}\cdot\phi$(0)	Convergence to Steady-State
1.0	6.0	1.0	I
1.0	5.5	1.0	II
2.0	5.5	1.0	I
2.0	5.0	1.0	II
3.0	5.0	1.0	I
3.0	4.5	1.0	II
4.0	4.0	1.0	I
4.0	3.5	1.0	II
5.0	3.0	1.0	I
5.0	2.5	1.0	II

4.3. Rate of Tumor Clearance

Another noted pattern in Figure 4.1 is a period of tumor suppression to a relatively negligible (but non-zero) level until $t \approx 80$ days. During this period, the tumor population is under the control of immunotherapy and the level of immune cells is relatively high. We can prolong this period of tumor suppression before the tumor population spikes and reaches its carrying capacity (at $t \approx 160$ in Figure 4.3) by simulating increased rates of tumor clearance (n_1 in Table 2.1 by CAR-T cells and immune cells. Realistically, this could be achieved by artificially increasing the affinity of the chimeric antigen receptors of CAR-T cells for the antigens expressed by the tumor cells, through different laboratorial approaches which will be discussed in the next section.

Figure 4.4 compares the dynamics of two systems with different rates of tumor clearance, showing that the tumor is inhibited for approximately twice as long under immune surveillance with a

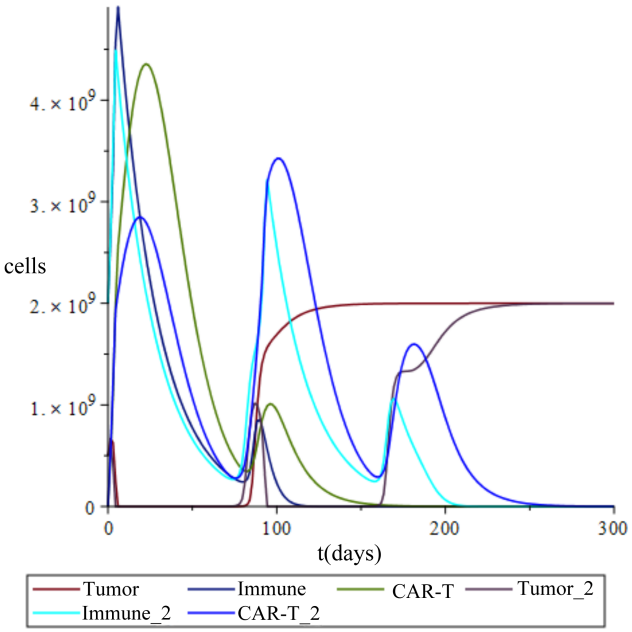

FIGURE 4.3. Tumor immune dynamics. Increasing the rate of tumor clearance from n_1 = 0.1245 to 0.15 allows the host to survive for a longer period of time. The lines labeled "2" represent the system with increased tumor clearance where the tumor population takes approximately double the time to reach the carrying capacity.

higher rate of clearance ($t \approx 80$ with $n_1 = 0.1245$ and $t \approx 160$ with $= 0.15$) before it proliferates if the CAR-T cells and immune cells are more efficient at killing the tumor. While not visualized, we also obtain faster suppression of tumor populations by CAR-T and immune cells in equilibrium (II) given a higher rate of tumor clearance; this could potentially lead to a shortened therapy. Based on the pattern, we conclude that CAR-T treatment can improve the life expectancy of cancer patients with either higher specificity for the targeted tumor population or higher responsiveness to the tumor antigens.

4.4. Injecting CAR-T

We now turn our attention to the injection of CAR-T cells which, initially assumed to be none, can also be controlled as a human factor in this model. By substituting a logistic growth model into p_2 (refer to Table 2.1), we can control the amount of CAR-T cells injected into the system and the time at which the injection initiates. The function we substitute for the injection rate is

$$p_2(t) = \frac{6.5 \times 10^7}{1 + e^{(a-t)}} \tag{4.1}$$

where a represents the time at which the injection initiates and 6.5×10^7 represents the amount of CAR-T cells injected per day. Due to the new system no longer being autonomous with a function of t on the RHS of the differential equations, the equilibria will not be analyzed. However, using graphical analysis, we observe different outcomes in tumor response to CAR-T immunotherapy by comparing different times of injection while keeping other factors constant. Figure 4.5 is a visualization of the response of the tumor population over time.

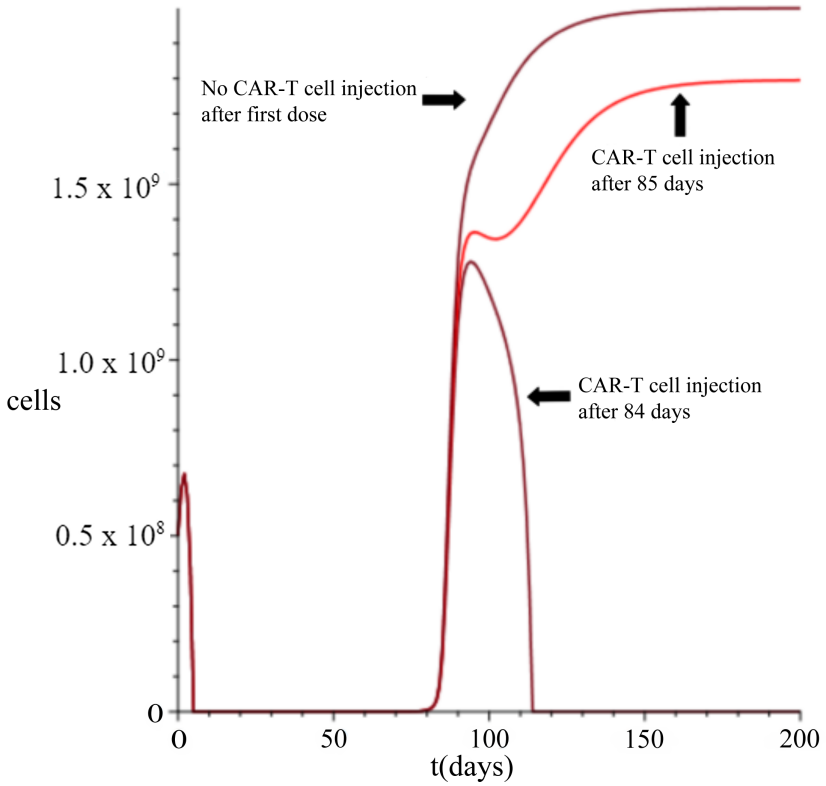

FIGURE 4.4. Effect of CAR-T injection on tumor population. Three lines showing the outcomes of tumor population in response to CAR-T injection at different times. The tumor is successfully eliminated by CAR-T cells if the injection happens before day 85, after which the tumor will persist and out-compete immunotherapy.

A constant rate of CAR-T injection is set at $6.5 \times 10^8\ cells\ day^{-1}$, and after simulating with different starting times of the injection, remarkably disparate outcomes are obtained over a one-day difference at t = 84 and 85. With CAR-T injection beginning at day 84 or earlier, the tumor is successfully controlled by the therapy, while with injection beginning after day 85, the tumor proliferates after a temporary suppression at $t \approx 100$ and approaches its carrying capacity, leading to health deterioration of the host. This provides substantial support for the importance of the time frame of cancer treatment with CAR-T immunotherapy by showing that a delayed secondary therapy will be less likely to successfully control the tumor growth within the host.

5. Extended Model

In the last part of this paper, we now consider an extended version of the system, with the introduction of host cells (H). This extension is made to account for the off-target toxicity of CAR-T cells, as the therapy is known to have side effects affecting the body (León-Triana et al., 2021). The extra terms included are designed to model the inhibition of tumor cells by host cells via defense mechanisms at rate γ (in (5.1)), the activation of immune cells by host cells through antigen presenting at rate δ (in (5.2)), logistic growth of host cells at rate p_3 (adopted from Das et al. (2020)) and carrying capacity κ_4, destruction of host cells by tumor cells at rate K_3, and lastly the effect of CAR-T toxicity on host cells at rate K_4 (in (5.4)) (Das et al., 2020).

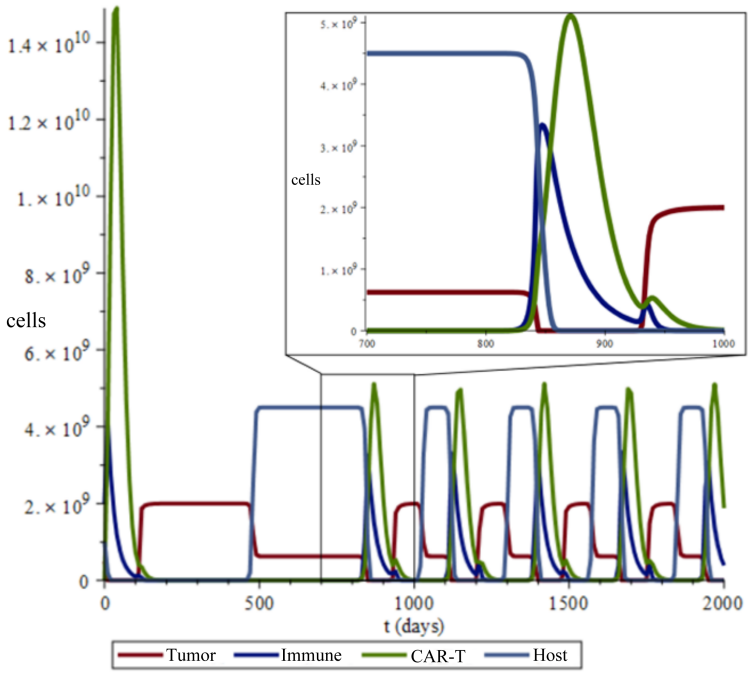

FIGURE 5.1. Oscillating dynamics of host, tumor, immune and CAR-T. The oscillating relationships show competition between the populations due to inhibitory effects. Parameters used in this graph that are not in Table 3.1 are $\gamma = 1.5\times10^{-10}, \delta = 2.5 \times 10^{-11}, p_3 = 0.5, \kappa_4 = 5 \times 10^9, K_3 = 8.0 \times 10^{-11}, K_4 = 3 \times 10^{-10}$. All are estimated for numerical simulation.

$$\frac{dT}{dt} = \alpha T(\ln\beta - \ln T) - \frac{n_1 T(M+\phi)}{T+\kappa_1} - \gamma HT \tag{5.1}$$

$$\frac{dM}{dt} = \frac{n_2 TM}{T+\kappa_2} - p_1 M - K_1 TM + \delta HM \tag{5.2}$$

$$\frac{d\phi}{dt} = p_2 + \frac{n_3 TM}{T+\kappa_3} - \frac{1}{\tau_c}\phi + K_2\phi M \tag{5.3}$$

$$\frac{dH}{dt} = p_3 H\left(1 - \frac{H}{\kappa_4}\right) - K_3 TH - K_4\phi H. \tag{5.4}$$

A different set of parameters are used to numerically simulate this model, with $p_1 = 0.5, p_2 = 8 \times 10^{-11}, p_3 = 9 \times 10^{-10}, \alpha = 1.5 \times 10^{-10}$. Observation of an oscillating pattern is obtained, involving competition between the four populations as shown by Figure 5.1.

The oscillation, when compared to the steady-state equilibria of the three-equation system, demonstrates that CAR-T toxicity impacts the healthy host cells to certain degrees by showing the lack of stability and cooperation between the host cells and CAR-T cells. To investigate whether stability exists in this system, the Jacobian matrix of the system is obtained using the parameters:

$$\mathbf{Jacobian} = \begin{bmatrix} J_{11}, J_{12}, J_{13}, J_{14} \\ J_{21}, J_{22}, J_{23}, J_{24} \\ J_{31}, J_{32}, J_{33}, J_{34} \\ J_{41}, J_{42}, J_{43}, J_{44} \end{bmatrix} \tag{5.5}$$

where,

$$J_{11} = 0.580 \ln\left(\frac{2 \cdot 10^9}{T}\right) - 0.580 - \frac{0.1245 \cdot (M+\phi)}{T + 2.019 \cdot 10^7} + \frac{0.1245 \cdot T \cdot (M+\phi)}{(T + 2.019 \cdot 10^7)^2} - 1.5 \cdot 10^{-10} \cdot H \tag{5.6}$$

$$J_{12} = \frac{-0.1245 \cdot T}{(T + 2.019 \cdot 10^7)} \tag{5.7}$$

$$J_{13} = \frac{-0.1245 \cdot T}{(T + 2.019 \cdot 10^7)} \tag{5.8}$$

$$J_{14} = -1.50 \cdot 10^{-10} \cdot T \tag{5.9}$$

$$J_{21} = \frac{0.35 \cdot M}{T + 3.50 \cdot 10^7} - \frac{0.35 \cdot T \cdot M}{(T + 3.50 \cdot 10^7)^2} - 3.40 \cdot 10^{-10} \cdot M \tag{5.10}$$

$$J_{22} = \frac{0.35 \cdot T}{T + 3.50 \cdot 10^7} - 0.042 - 3.40 \cdot 10^{-10} \cdot T + 2.50 \cdot 10^{-11} \cdot H \tag{5.11}$$

$$J_{23} = 0 \tag{5.12}$$

$$J_{24} = 2.50 \cdot 10^{-11} \cdot M \tag{5.13}$$

$$J_{31} = \frac{0.1 \cdot M}{T + 1 \cdot 10^7} - \frac{0.12 \cdot T \cdot M}{(T + 1.0 \cdot 10^7)^2} \tag{5.14}$$

$$J_{32} = \frac{0.12 \cdot T}{T + 1.0 \cdot 10^7} + 4.92 \cdot 10^{-11} \cdot \phi \tag{5.15}$$

$$J_{33} = \frac{-1}{14} + 4.92 \cdot 10^{-11} \cdot M \tag{5.16}$$

$$J_{34} = 0 \tag{5.17}$$

$$J_{41} = \frac{-H}{1.25 \cdot 10^{10}} \tag{5.18}$$

$$J_{42} = 0 \tag{5.19}$$

$$J_{43} = \frac{-9 \cdot H}{10^{10}} \tag{5.20}$$

$$J_{44} = 0.5 - 2.00 \cdot 10^{-10} \cdot H - \frac{T}{1.25 \cdot 10^{10}} - \frac{9 \cdot \phi}{10^{10}}. \tag{5.21}$$

We also solve for the steady-states and obtain the eigenvalues of the 4 steady-states (out of the 30 total solutions) that are biologically relevant using the same method as mentioned in the analysis section.

$$\text{(I)}\{T = 2.000 \times 10^9, M = 0, \phi = 0, H = 0\} \tag{5.22}$$

$$\text{(II)}\{T = 6.245 \times 10^8, M = 0, \phi = 0, H = 4.500 \times 10^9\} \tag{5.23}$$

$$\text{(III)}\{T = 4.993 \times 10^6, M = 3.972 \times 10^8, \phi = 3.059 \times 10^8, H = 0\} \tag{5.24}$$

$$\text{(IV)}\{T = 8.658 \times 10^8, M = 7.656 \times 10^8, \phi = 2.690 \times 10^9, H = 0\}. \tag{5.25}$$

There is one tumor-dominant equilibrium (I), two host cell-free equilibria (III) and (IV), and one immune-CAR-T free equilibrium (II). Their eigenvalues and stability are listed respectively, as followed.

$$\text{(I)}\ [-0.5800, -0.3780, -0.07142, 0.3400] \tag{5.26}$$

$$\text{(II)}\ [0.1896, -0.07143, -0.3202, -0.7098] \tag{5.27}$$

$$\text{(III)}\ [0.2243, 0.05916 + 0.3495 \cdot i, -0.06105, 0.05916 - 0.3495 \cdot i] \tag{5.28}$$

$$\text{(IV)}\ [0.2023, -0.1708 + 0.1157 \cdot i, -1.990, -0.1708 - 0.1157 \cdot i]\,. \tag{5.29}$$

All four sets of eigenvalues have mixed signs, and two of them involve imaginary numbers. The eigenvalues of the four equilibria show that none of systems are asymptotically stable. Rather than converging to constants steady-states, the populations will only enter oscillating states as seen in Figure 5.2, regardless of the starting populations. An additional suggestion of competition within the extended model also comes from the comparison of the outcome to the predatory-prey Lotka-Volterra model, where similar oscillation is observed between predator and prey populations. The conclusion we can draw from this model is limited as this extended model needs further analysis of steady-state behavior: we are only able to obtain a number of unstable nodes from this system using estimated parameters, which doesn't provide support for the coexistence of cell populations based on the model. Further modifications, which are discussed in the next section, are needed to more accurately describe the sustainability of the relationship between the host and CAR-T treatment while accounting for more possible factors that could affect the success of the treatment.

6. Conclusion

In this study, differential equations are introduced to model the relationship between tumor, immune, and CAR-T cell populations based on the rates of change. Using these equations, different parameters are tested to understand how the relationship between the three cell types is affected based on certain conditions. These conditions are then used to find the steady states and stability of the equations based on the Jacobian matrix of the system. Different scenarios are presented where the tumor, immune, and CAR-T cells maintained stable populations through the steady states. Through in silico testing of different values for parameters, it is shown that the time between CAR-T injections can play a major role in a host surviving, increasing tumor clearance can help a host survive longer with a tumor, and a host can survive while possessing tumors under certain conditions.

After analyzing the data, it is clearly shown that the efficiency of CAR-T treatment is affected by certain parameters. One insight of this study is that early action is critical in two phases of cancer treatment. The first is tumor detection. The analysis shows that CAR-T therapy can successfully control an initial tumor population of 10^8 cells, but not a population of 5×10^8 cells. Realistically, a lower initial tumor population corresponds to an earlier detection of the tumor in the body. In

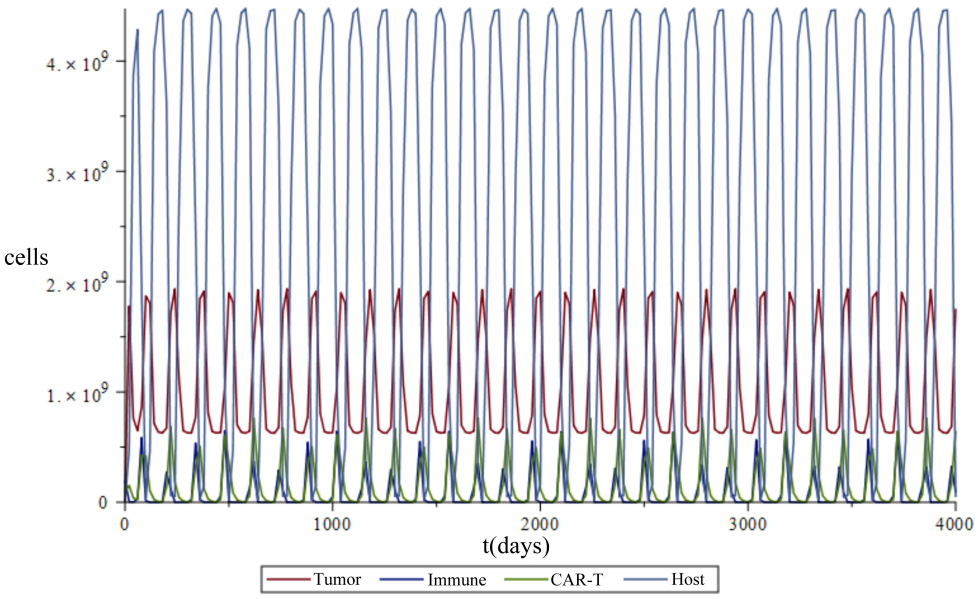

FIGURE 5.2. Oscillating dynamics of host, tumor, immune and CAR-T. Oscillation starts almost immediately with initial values closer to the equilibrium values of steady-state (III) of the extended system. Initial values are $\{T(0) = 5 \cdot 10^6, M(0) = 2 \cdot 10^8, \phi(0) = 10^8, H(0) = 10^7\}$.

order for a successful CAR-T therapy to be applied, a tumor size of less than around 5×10^8 cells is necessary with the parameters used in the calculations. With more frequent screening for tumors in the body, many patients can experience more successful treatments based on this conclusion.

The strength of the host's immunity is also a factor that influences the system. With a larger $M(0)$, or amount of immune cells initially present in the host, the tumor will more likely be suppressed. The relationship between the initial immune and tumor cell count is modeled in this study, and a function is applied to fit the minimal host immunity to suppress different tumor sizes temporarily. From this, we draw the reasonable conclusion that individuals with very weak immunity, such as patients of auto-immune diseases or the immuno-compromised may not be suitable for CAR-T treatment, because the therapy wouldn't be able to produce enough synergistic effect with the severely weakened immune system to successfully put the tumor population under control. However, this doesn't mean that other types of treatment, such as chemotherapy, are unavailable to such patients.

A second critical phase of CAR-T treatment is injection time. In treating many different diseases, relapses are frequently countered by continuous or periodic treatment. Based on the model, we found a critical time frame before which a continuous CAR-T treatment must begin to prevent the relapse of the tumor. While the time frame varies with the amount of injection applied, for a continuous CAR-T injection of 6.5×10^7 cells per day, we found that a continuous treatment is required to begin before day 84 after the initial CAR-T therapy, otherwise, the tumor population will be able to out-compete the immune cells and overcome the CAR-T therapy. For different amounts of CAR-T cells injected per day, the critical moment may differ significantly. Modeling the relationship between the amount of injection and the time frame of tumor suppression is a valuable subject of further research, and the finding may impose limitations on the practical application of CAR-T treatment.

CAR-T treatment can also be improved in the laboratory. With an increased affinity for tumor antigens, CAR-T cells would have increased rates of tumor clearance, which, as shown by the analysis and numerical simulations, leads to improvement of the treatment efficiency by prolonging the period of tumor suppression in patients. This conclusion points to multiple directions to improve the therapeutic effect of CAR-T immunotherapy. Genetic recombination of engineered receptors that are more affinitive or specific to tumor antigens can prevent tumor cells from evading detection and destruction. Some previously unnoticed tumor antigens may also be exploited by chimeric antigen receptors to achieve similar objectives and potentially prevent some off-target CAR-T attacks. The longer lifespan of CAR-T cells can allow them to persist in the host system longer and improve their activities. Chemical treatment can be combined with CAR-T cells as a means of control and activity boost for tumor destruction... These subjects are all of interest for further research despite belonging to different fields, and improvement of CAR-T therapy will bring us further to the solution of cancer as a global health problem.

Another subject of further research proposed in this study is often overlooked. To reiterate a previous point, CAR-T cells are known to not be side-effect free, and during clinical applications, toxic responses have been recorded in patients, leading to compromises in the outcome of the therapy. In the end, in section 4 we proposed a four-equation system based on our original model to account for the toxic effect of CAR-T cells on an off-target host cell population. Preliminary stability analysis and numerical simulations conducted yield an oscillating pattern between the four populations with a lack of stability in the four steady states, which directs future research to investigate the pattern of coexistence within four cell populations. Potential approaches include further modifications to the model and analysis of parameters to find values that would provide stability based on the Routh-Hurwitz criteria. While this topic isn't thoroughly discussed in this paper, future research may built on this extended model and produce significant results regarding the severity and toxicity of CAR-T therapy and whether that poses challenges to clinical applications of cancer treatment.

Acknowledgments

The student authors would like to thank the North Carolina Summer Ventures Program and faculty instructors at University of North Carolina Wilmington for the opportunity and support on this research project.

References

S. Bahrambeigi, D. Sanajou, and V. Shafiei-Irannejad. Major fundamental factors hindering immune system in defense against tumor cells: the link between insufficiency of innate immune responses, metabolism, and neurotransmitters with effector immune cells disability. *Immunology Letters*, 212:81–87, 2019.

L. R. Barros, E. A. Paixão, A. M. Valli, G. T. Naozuka, A. C. Fassoni, and R. C. Almeida. CART math - A mathematical model of CAR-T immunotherapy in preclinical studies of hematological cancers. *Cancers*, 13(12):2941, 2021.

CDC. Cancer data and statistics. `https://www.cdc.gov/cancer/uscs/`, 2022. Retrieved July 18, 2022.

P. Das, P. Das, and S. Mukherjee. Stochastic dynamics of Michaelis–Menten kinetics based tumor-immune interactions. *Physica A: Statistical Mechanics and its Applications*, 541:123603, 2020.

A. d'Onofrio, A. Fasano, and B. Monechi. A generalization of Gompertz law compatible with the Gyllenberg–Webb theory for tumour growth. *Mathematical Biosciences*, 230(1):45–54, 2011.

L. Edelstein-Keshet. *Mathematical models in biology*. SIAM, 2005.

C. S. Holling. Some characteristics of simple types of predation and parasitism. *The Canadian Entomologist*, 91(7):385–398, 1959.

M. Itik and S. P. Banks. Chaos in a three-dimensional cancer model. *International Journal of Bifurcation and Chaos*, 20(01):71–79, 2010.

A. L. Jenner, P. S. Kim, and F. Frascoli. Oncolytic virotherapy for tumours following a gompertz growth law. *Journal of Theoretical Biology*, 480:129–140, 2019.

V. A. Kuznetsov, I. A. Makalkin, M. A. Taylor, and A. S. Perelson. Nonlinear dynamics of immunogenic tumors: parameter estimation and global bifurcation analysis. *Bulletin of Mathematical Biology*, 56(2):295–321, 1994.

O. León-Triana, A. Pérez-Martínez, M. Ramírez-Orellana, and V. M. Pérez-García. Dual-target CAR-Ts with on-and off-tumour activity may override immune suppression in solid cancers: A mathematical proof of concept. *Cancers*, 13(4):703, 2021.

G. E. Mahlbacher, K. C. Reihmer, and H. B. Frieboes. Mathematical modeling of tumor-immune cell interactions. *Journal of Theoretical Biology*, 469:47–60, 2019.

A. Marino-Enriquez and C. D. Fletcher. Shouldn't we care about the biology of benign tumours? *Nature Reviews Cancer*, 14(11):701–702, 2014.

V. M. Pérez-García, O. León-Triana, M. Rosa, and A. Pérez-Martínez. CAR T cells for T-cell leukemias: Insights from mathematical models. *Communications in Nonlinear Science and Numerical Simulation*, 96:105684, 2021.

P. Queirolo, A. Boutros, E. Tanda, F. Spagnolo, and P. Quaglino. Immune-checkpoint inhibitors for the treatment of metastatic melanoma: a model of cancer immunotherapy. *Seminars in Cancer Biology*, 59:290–297, 2019.

M. Robertson-Tessi, A. El-Kareh, and A. Goriely. A mathematical model of tumor–immune interactions. *Journal of Theoretical Biology*, 294:56–73, 2012.

B. Srinivasan. A guide to the Michaelis–Menten equation: steady state and beyond. *The FEBS journal*, 2021.

T. Uehara, H. Yoshida, K. Tate, and T. Kato. Metachronous occurrence of two different histological subtypes of endometriosis-related neoplasms. *Gynecologic Oncology Reports*, 27:42–45, 2019.

C. Vaghi, A. Rodallec, R. Fanciullino, J. Ciccolini, J. P. Mochel, M. Mastri, C. Poignard, J. M. Ebos, and S. Benzekry. Population modeling of tumor growth curves and the reduced Gompertz model improve prediction of the age of experimental tumors. *PLoS Computational Biology*, 16 (2):e1007178, 2020.

B. Xie, Z. Zhang, and N. Zhang. Influence of the fear effect on a Holling type II prey–predator system with a Michaelis–Menten type harvesting. *International Journal of Bifurcation and Chaos*, 31(14):2150216, 2021.

A. Yates and R. Callard. Cell death and the maintenance of immunological memory. *Discrete & Continuous Dynamical Systems-B*, 1(1):43, 2001.

(E.J. Xie) GREEN HOPE HIGH SCHOOL, CARY, NC 27519, USA

(H. Ramasamy) ARDREY KELL HIGH SCHOOL, CHARLOTTE, NC 28277, USA

(W. Feng) DEPARTMENT OF MATHEMATICS AND STATISTICS, THE UNIVERSITY OF NORTH CAROLINA AT WILMINGTON, WILMINGTON, NC 28403, USA

Email address, Corresponding author: fengw@uncw.edu